**Turkish Computational and Theoretical Chemistry**

*Turkish Comp Theo Chem (TC&TC)*

***Volume(Issue): 5(2) – Year: 2021 – Pages: 35-45***

***e-ISSN: 2602-3237***

***https://doi.org/10.33435/tcandtc. 1018412***

***Received:*** 03.11.2021 ***Accepted:*** 08.12.2021 *Research Article*

# *Methyl-mercaptane adsorption and sensing on Fe-/Co-graphene structures: A DFT study*

**Numan Yuksel[a], Ahmet Kose[a], M. Ferdi Fellah [1,a]**

[a] Department of Chemical Engineering, Bursa Technical University, Mimar Sinan Campus, 16310, Bursa, Turkey.

**Abstract:** In this research, the adsorption and detection abilities of Fe and Co doped graphene structures for methyl-mercaptan molecule were investigated by Density Functional Theory (DFT) method. B3LYP hybrid functional and LANL2DZ/6-31G(d,p) basis sets were used in the calculations. At the end of the adsorption processes, Fe and Co doped graphene structures were determined to be suitable adsorbents for the methyl-mercaptan molecule. In addition, charge transfer happened from the methyl-mercaptan molecule to the Fe and Co-doped graphene structures. The electronic sensor and the Φ-type sensor properties were also investigated and it was determined that Fe-graphene structure could be only used as an electronic sensor for methyl-mercaptan molecule at room temperature.

***Keywords:*** *DFT, methyl-mercaptane, graphene, adsorption, sensor*

## 1. Introduction

One of the main causes of environmental pollution caused by the consumption of fossil fuels is sulfur compounds. Since sulfuric compounds cause acid rain, air pollution and depletion of the ozone layer, removal of sulfur compounds is of great importance. At the same time, the concentrations of these compounds should be kept at limit values in order to prevent their harm to human health [1-3]. Methyl-mercaptane (MM), one of the sulfur compounds, is one of the volatile organic compounds known for its unpleasant odor. It is added to natural gas because it has a very low odor threshold, and it can also be encountered in waste water treatment, in the food industry, in waste fields. MM is an important volatile compound that seriously harms human health as well as environmental pollutants. MM shows significant adverse effects on human health even at very low exposure doses such as 10 ppm. For this reason, the adsorption and detection of MM is of great importance. [4-8]. In this respect, investigation of the adsorption and sensor properties of MM has focused on boron nitride nanosheet, zeolite and graphene materials [1,8,9].

Graphene is one of the materials that attract attention in environmental protection applications with its features such as low cost, high surface area and high surface/volume ratio. Additionally, its highly stable structure, low contamination and ease of processing facilitate gas adsorption on its surfaces [10,11]. When graphene is used as a chemical sensor, it provides high conductivity and ballistic transport with little signal degradation at ambient temperature [12]. Hidalgo et al. have found that MM can be adsorbed physically on graphene using the DFT method [13]. In order to improve the adsorption and sensing ability of graphene, it is functionalized with transition metal atoms. The added metal atoms change the electronic structure of graphene, improving the interaction between gas molecules and graphene, and the sensing ability of graphene increases significantly [14-15]. Shahmoradi et al. found that MM has a weak adsorption energy value (-0.022 kJ/mol) on pure graphene by DFT method. It is noteworthy that the

[1] Corresponding Authors

e-mail: mferdi.fellah@btu.edu.tr

interaction of MM with graphene increased significantly when they decorated the graphene with Ni and Pt atoms [16]. Although noble metals show good catalyst properties for gas adsorption, non-noble metals attract attention with their low cost and excellent detection properties [17]. In the study done by doping various elements on graphene, it was explained that the structures of Fe and Co doped graphene have high binding energy for another sulfide molecule, $H_2S$, and that Fe doped graphene greatly improves the sensor ability compared to pure graphene [18]. In this research, the adsorption and detection abilities of MM on Fe and Co doped graphene structures were investigated by DFT method.

## 2. Computational Method

The theoretical computations employed in present study were based on DFT [19] used in Gaussian 09 software [20]. The method applied here for DFT calculations was the B3LYP hybrid method considering the effects of exchange and correlation [21,22]. For iron and cobalt atoms, the LanL2DZ basis set was utilized. The graphene sheet structure modeled as the cluster with 73 carbons has been used in this research. Hydrogen (H) atoms have been attached to the ends of the bonds of the free carbon atoms of the plate. In this study, all atoms were kept relaxed during the theoretical computations. The 6-31G (d,p) basis set has been utilized for carbon and hydrogen atoms. The energy values include zero-point energy (ZPE) corrections. These values have been calculated at atmospheric pressure (1 atm) and room temperature (298.15 K). The Fe and Co doped graphene structures and MM molecule were optimized structurally (to obtain equilibrium geometry (EG)). Here, Fe and Co atoms were doped instead of the central carbon atom of the graphene cluster. The adsorption energy values were computed by following equations in Gaussian09.

$$E = ZPE + E_{electronic} + E_{vibrational} + E_{translational} + E_{rotational} \quad (1)$$

$$H = E + RT \quad (2)$$

$$G = H - TS \quad (3)$$

$$\Delta(E / H / G) = (E / H / G)_{System} - [(E / H / G)_{Adsorptive} + (E / H / G)_{Doped\ Graphene} \quad (4)$$

$$\text{Chemical-hardness value } (\eta) = \frac{I-A}{2} \quad (5)$$

$$\text{Chemical-potential value } (\mu) = -\frac{I+A}{2} \quad (6)$$

$$\text{Electronegativity value } (\chi) = -\mu \quad (7)$$

$$\text{Electrophilicity value } (\omega) = \frac{\mu^2}{2\eta} \quad (8)$$

here $I \approx -\epsilon_{HOMO}$ and $A \approx -\epsilon_{LUMO}$

E equals to the sum of the electronic, ZPE, and thermal energies, H equals to the sum of the thermal energies and enthalpy, G equals to the sum of thermal enthalpy and free energy, T is the temperature, S is the entropy, and R is the global ideal gas constant. The following equation was utilized to calculate the relative adsorption energy, adsorption enthalpy, and adsorption Gibbs free energy values.

Here system means Fe-doped graphene and Co-doped graphene structures with adsorbate, adsorptive is adsorbing molecule and cluster is Fe- and Co-graphene clusters. The HOMO (Highest Occupied Molecular Orbital) and LUMO (Lowest Unoccupied Molecular Orbital) energy values were computed by full population analysis. Besides, chemical hardness, chemical potential, electronegativity, electrophilicity, HOMO ($\epsilon_{HOMO}$) and LUMO ($\epsilon_{LUMO}$) energies were calculated by

next equations which are based on Koopmans approach [23,24].

The convergence criteria applied in DFT calculations utilized in Gaussian software are $18x10^{-4}$ bohr for max displacement, $12x10^{-4}$ radian for gradients of root-mean-square (rms) displacement, $45x10^{-5}$ hartree/bohr for max force and $3x10^{-4}$ hartreee/radian for rms force during DFT computations utilized in this study. In addition, the SCF convergence criteria applied in DFT calculations utilized in Gaussian software for rms change in the density matrix and maximum change in the density matrix were $1x10^{-8}$ and $1x10^{-6}$, respectively. Gausssum software [25] has been used to obtain the density of states (DOS). Mulliken atomic charges of atoms [26] has been found by using the Mulliken population analysis. In addition, the graphs for electron localization function (ELF) were obtained by using Multiwfn software [27].

## 3. Results and discussion

Firstly, the metal-doped graphene structures have been optimized geometrically. The optimized Fe- and Co-graphene clusters are shown in Fig. 1. After the MM molecule has also been optimized adsorption of MM molecule has been studied on the optimized Fe and Co doped graphene structures. The MM adsorbed metal-doped graphene structures are shown in Fig. 2. The adsorption energy values for MM on Fe- and Co-graphene structures have been listed in Table 1. According to adsorption energy (ΔE) and adsorption entalphy (ΔH) values, negative values were obtained for both structures after MM adsorption. Negative ΔH values indicate that the process is exothermic. It has been revealed that adsorption processes can occur spontaneously on both Fe-graphene and Co-graphene structures due to negative Gibbs free energy change (ΔG) values. The adsorption energy on Co-graphene structure is lower than that on Fe-doped graphene structure. Accordingly, as expected the bond distance of S-Fe (2.539 Å) is higher than the bond distance of S-Co (2.531 Å).

**Table 1** The adsorption energies of the MM molecule on Fe- and Co-graphene structures (unit of the values here is kJ/mol).

| Structure | ΔE | ΔH | ΔG |
|---|---|---|---|
| Fe-graphene | -45.8 | -48.3 | -4.6 |
| Co-graphene | -47.6 | -50.0 | -6.3 |

Two parameters were generally utilized to investigate the sensitivity of the electrical characteristics of Fe- and Co-graphene structures to the MM molecule. The parameters to be investigated here are the workfunction (Φ) and the energy gap between HOMO and LUMO (Eg). The Eg values of Fe- and Co-graphene structure and MM adsorbed Fe- and Co-graphene structure are accepted as follows:

$$E_g = \in_{LUMO} - \in_{HOMO} \qquad (9)$$

$E_g$ has been shown to be a reliable predictor of nanosensor sensitivity measurements on numerous occasions [28,29]. The adsorption of an adsorbate causes a change in electrical conductivity (σ), which is how a chemical sensor works. The following relationship between $E_g$ and σ has been determined [30,31].

$$\sigma = AT^{\frac{3}{2}} \exp\left[\frac{-E_g}{2\kappa T}\right] \qquad (10)$$

Here κ is the Boltzmann's constant, A which has the unit of *electrons/m$^3$K$^{3/2}$* is a constant value and T is temperature. Several studies have shown that the results of laboratory tests back up the findings of using this equation [32,33]. The reduction in $E_g$ raises the population of conduction electrons exponentially, according to Eq. (10). As a result of the chemical present in the environment, there is an increase in electrical conductivity. Adsorption of a component alters the workfunction (Φ) value of the sensor, which moves the gate voltage, generates an electrical signal, and assists chemical recognition [34]. The amount of energy required to remove an electron from the Fermi level is known as Φ [35].

$$\Phi = Vel(+\infty) - E_F \qquad (11)$$

Here $E_F$ equals to the energy of Fermi level and $V_{el}(+\infty)$ equals to the electrostatic potential energy of the electron located far from the surface of material. The value of $V_{el}(+\infty)$ was then taken to be zero [33,34]. Assuming the $V_{el}(+\infty)$ and $\Phi$ values equivalent to zero and $-E_F$, respectively. The following formula can be used to determine the $E_F$:

$$E_F = \in_{HOMO} + \frac{E_g}{2} = \in_{HOMO} + \frac{\in_{LUMO} - \in_{HOMO}}{2} = \frac{\in_{HOMO} + \in_{LUMO}}{2} \quad (12)$$

a)

b)

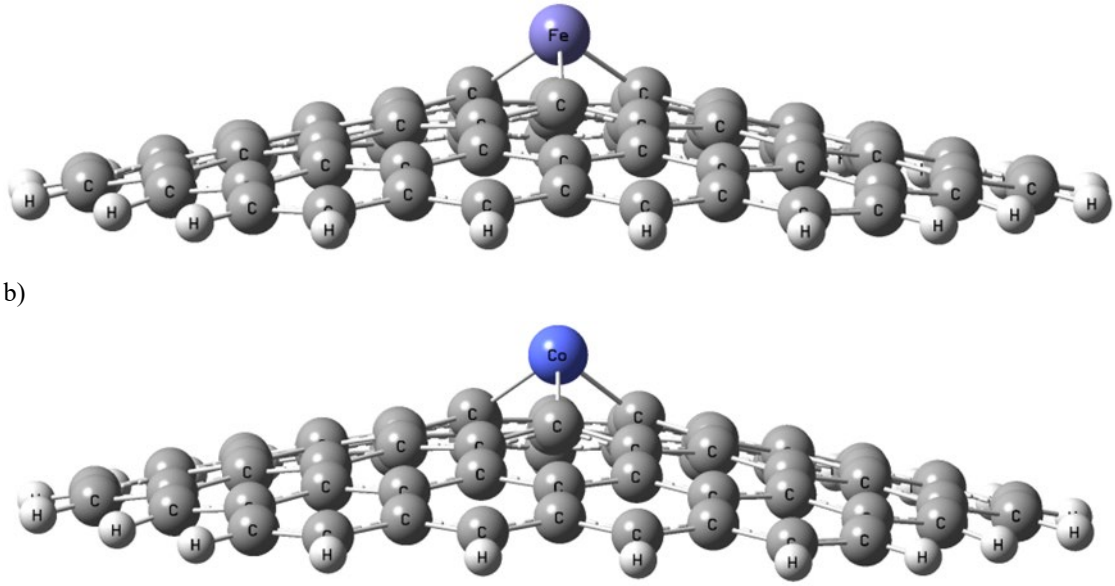


**Fig. 1** The geometries after optimization a) Fe-graphene structure and b) Co-graphene structure.

**Table 2** Electronic-properties of Fe- and Co-graphene structures and Fe- and Co-graphene/MM systems, including EF, Φ, HOMO and LUMO energies, Eg and ΔEg (unit of the values here is kJ/mol).
(After the MM adsorption, the ΔΦ% and ΔEg% represent the change in and Eg.)

| Structure | MOs | $E_{HOMO}$ | $E_{LUMO}$ | $E_g$ | $\Delta E_g$ | $\Delta E_g$% | Φ | ΔΦ% |
|---|---|---|---|---|---|---|---|---|
| Fe-graphene | α MOs | -381.8 | -198.9 | 182.8 | | | 290.4 | |
| | β MOs | -470.8 | -239.9 | 230.8 | | | 355.4 | |
| Fe-graphene/MM | α MOs | -372.6 | -195.8 | 176.8 | -6.0 | 3.3 | 284.2 | 2.1 |
| | β MOs | -460.7 | -285.4 | 175.3 | -55.5 | 24.0 | 373.1 | 4.9 |
| Co-graphene | α MOs | -375.9 | -194.1 | 181.8 | | | 285.1 | |
| | β MOs | -467.4 | -311.8 | 155.6 | | | 389.6 | |
| Co-graphene/MM | α MOs | -368.7 | -189.6 | 179.1 | -2.7 | 1.5 | 279.1 | 2.1 |
| | β MOs | -460.3 | -290.2 | 170.0 | 14.5 | 9.3 | 375.3 | 3.7 |

**Table 3** The values of η, μ, χ and ω for the optimized Fe- and Co-graphene structures and Fe- and Co-graphene/MM systems (unit of the values here is kJ/mol).

| Structure | MOs | η | μ | χ | ω |
|---|---|---|---|---|---|
| Fe-graphene | α MOs | 91.4 | -290.4 | 290.4 | 461.2 |
| | β MOs | 115.4 | -355.4 | 355.4 | 547.2 |
| Fe-graphene/MM | α MOs | 88.4 | -284.2 | 284.2 | 456.9 |
| | β MOs | 87.6 | -373.1 | 373.1 | 794.0 |
| Co-graphene | α MOs | 90.9 | -285.1 | 285.1 | 446.9 |
| | β MOs | 77.8 | -389.6 | 389.6 | 975.6 |
| Co-graphene/MM | α MOs | 89.6 | -279.1 | 279.1 | 434.9 |
| | β MOs | 85.0 | -375.3 | 375.3 | 828.2 |

a)

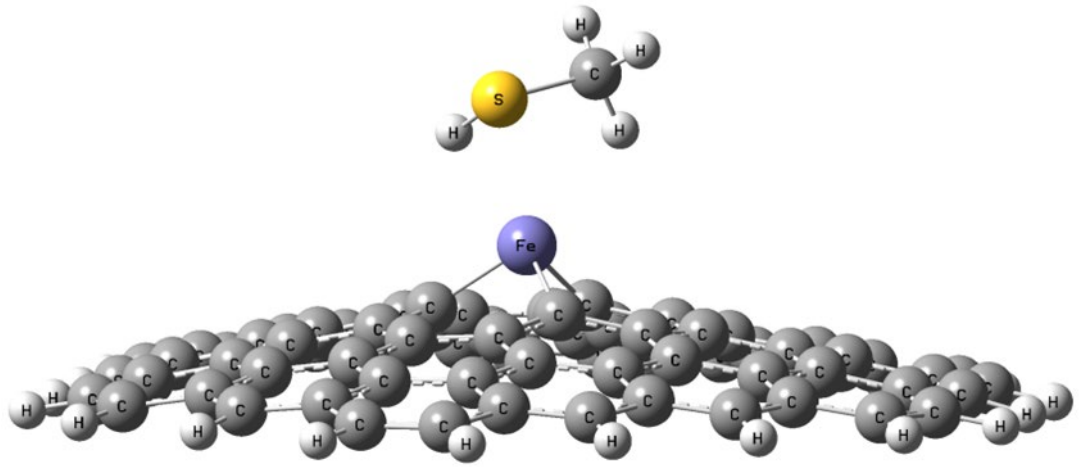


b)

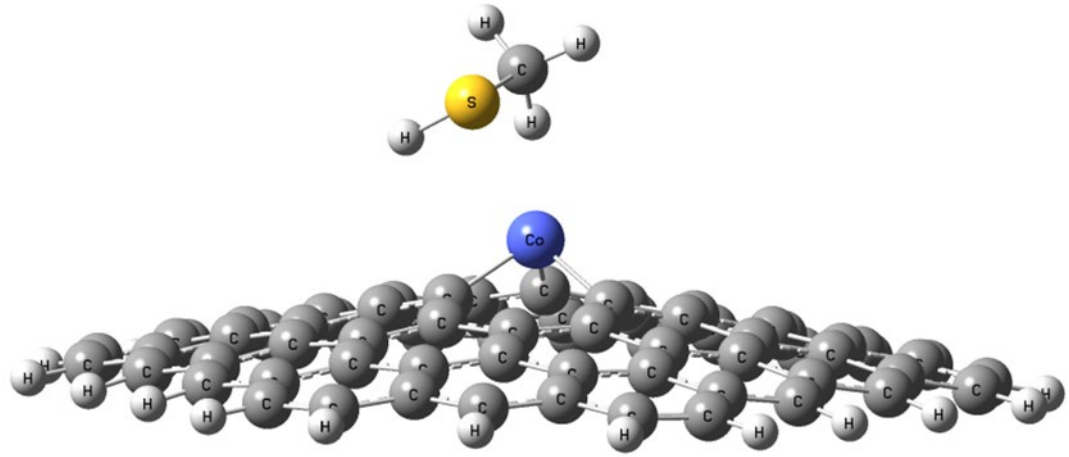


**Fig. 2** The geometries of the adsorbed MM after optimization on a) Fe-graphene structure and b) Co-graphene structure.

According to the results (Table 2), while Eg decreased in Fe-graphene structure, it increased for Co-graphene structure. Because the band gap of the Co-graphene structure does not decrease after adsorption, this structure can not be used as an electronic sensor. The Fe-graphene structure, on the other hand, has been found to be a useful electronic sensor due to its decreased Eg. For the Fe-graphene structure, 24% change in Eg was reached. Additionally, it has been determined that there is no Φ-type sensor feature since the change of work function for both structures is low. For both α molecular orbitals and β molecular orbitals (spin-up and spin-down respectively), chemical hardness (η), chemical potential (μ), electronegativity (χ), and electrophilicity (ω) values were computed and presented in Table 3.

The hardness of a chemical species is a measure of its resistance to changes in its electronic configuration. Along with electronegativity, it is considered a measure of chemical reactivity and stability. It's also been proposed that hard species interactions are essentially electrostatic, whereas soft species interactions are primarily covalent (i.e., through mixing of orbitals) [36]. According to the results in Table 3, it is seen that while the electronegativity of the Fe-graphene structure increases, the Co-graphene structure decreases. Thus, a stability difference emerged between the effect of these two atoms. In addition, it is seen that

while the hardness of the Fe-graphene structure decreases after adsorption, the Co-graphene structure increases. Accordingly, we can say that the interaction between the Fe-graphene structure and the MM molecule is covalent-based and the structure becomes softer, while the Co-graphene structure becomes harder and the interaction is electrostatically based. In present study, in order to acquire charge distribution after MM adsorption on Fe- and Co-graphene structures, the Mulliken population analysis have been utilized. After MM adsorption on the surface, MM's total charge was calculated in the Mulliken analysis as +0.23e, both systems. Here, it was revealed that the charge transfer after adsorption is from the MM molecule to the Fe- and Co-graphene structures. The HOMO-LUMO representations of Fe- and Co-graphene structures and all configurations of MM adsorbed Fe- and Co-graphene structures for α and β MOs have been illustrated in Fig. 3 and Fig. 4. In the HOMO-LUMO analysis, it is seen that LUMOs come to the fore in the interaction between the Fe- and Co-graphene structures and the MM molecule. In Fig. 3, the LUMOs concentrated in the electron-accepting part are located between the Fe atom and the MM molecule, especially in β MOs, after adsorption. This result refers to the Eg reduction occurring in β MOs. Looking at Fig. 4, LUMOs in β MOs prior to adsorption were concentrated around the Co atom, while after adsorption LUMOs disappeared from the interaction site. This refers to the increase of Eg in β MOs.

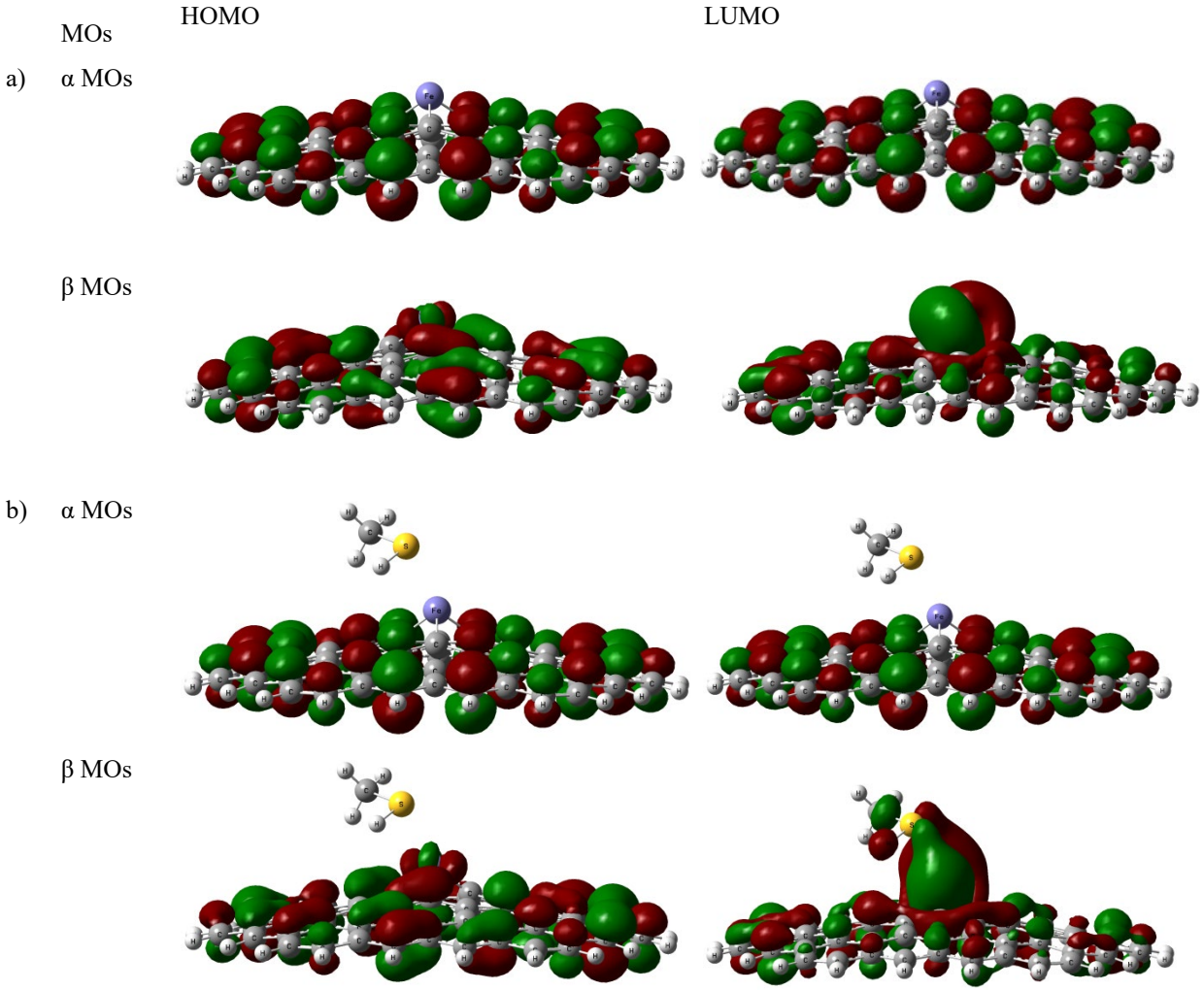


**Fig. 3** The representations for HOMO distributions and LUMO distributions of α molecular orbitals and β molecular orbitals for the optimized geometries of a) Fe-graphene structure and b) MM adsorbed on Fe-graphene structure.

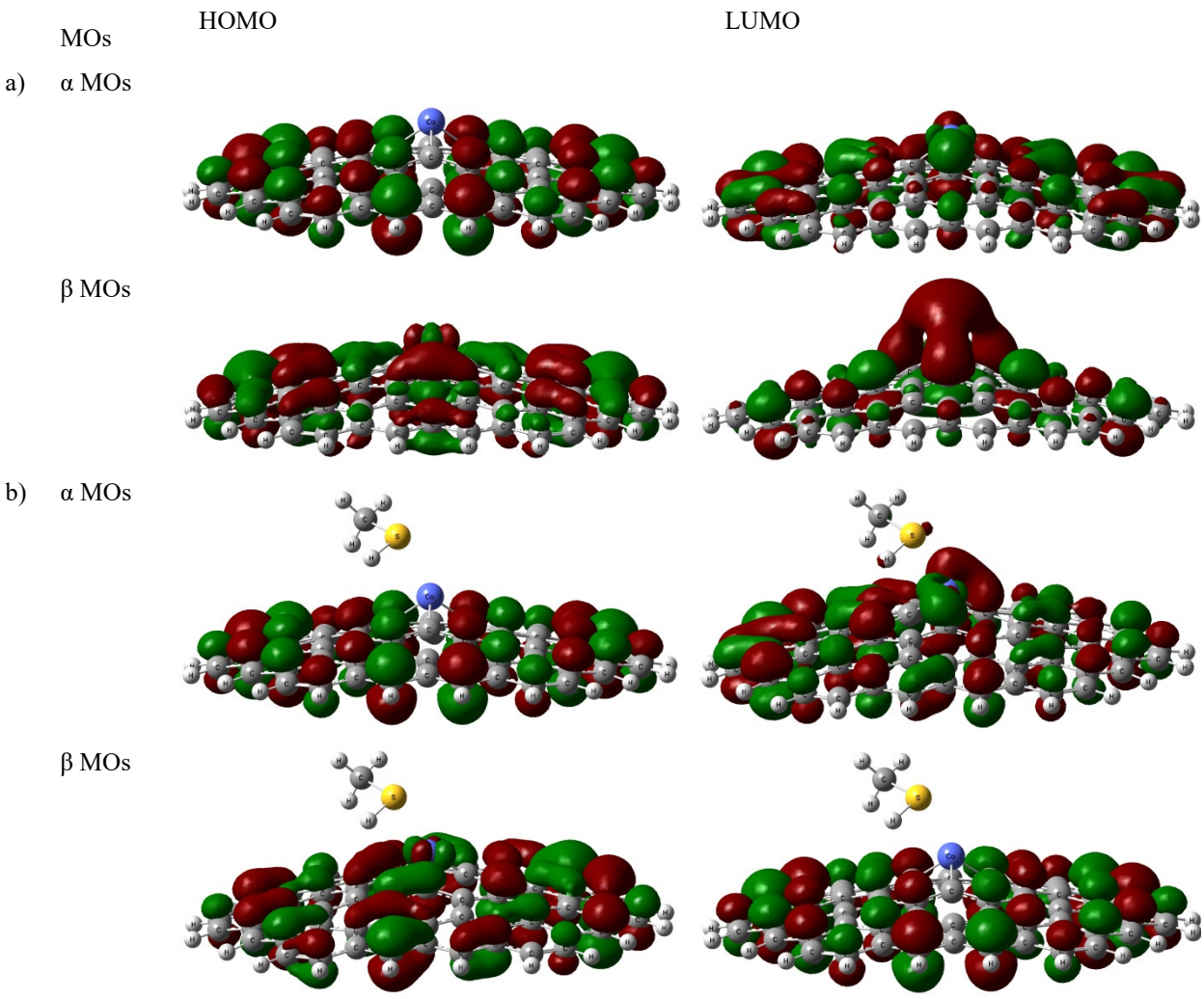


**Fig. 4** The representations for HOMO distributions and LUMO distributions of α molecular orbitals and β molecular orbitals for the optimized geometries of a) Co-graphene structure and b) MM adsorbed Co-graphene structure.

The density-of-states (DOS) of Fe- and Co-graphene structures and MM molecule adsorbed Fe- and Co-graphene structures have been presented in Fig. 5. It is seen that Eg reduces in Fe-graphene structure, whereas Eg increases in Co-graphene structure in β MOs. This means that the electrical conductivity of Fe-graphene structures increases whereas it reduces in Co-graphene structures.

Moreover, electrostatic potential distributions (ESP) for Fe- and Co-graphene structures and MM adsorbed Fe- and Co-graphene structures have been shown in Fig. 6. The positively and negatively regions of the Van der Waals surface were used to define blue and red colors on the ESP maps, respectively [37,38]. The ESP distributions are mapped to an electron density region with constant. The ESP increases by dissimilar colors so as to blue>green>yellow>red. As stated by the ESP analysis, we see that Fe and Co atoms form a blue zone on the graphene surface. Thus, we can say that metal atoms have a higher ESP and have more influence on the interaction than the graphene structure. In addition, after MM adsorption, we see that there is yellow color on the sulfur atom side of the MM molecule, whereas there is blue color on the methyl group. If we consider the electron donor property of the methyl group [39], we can guess that the methyl group has a say in charge transfer.

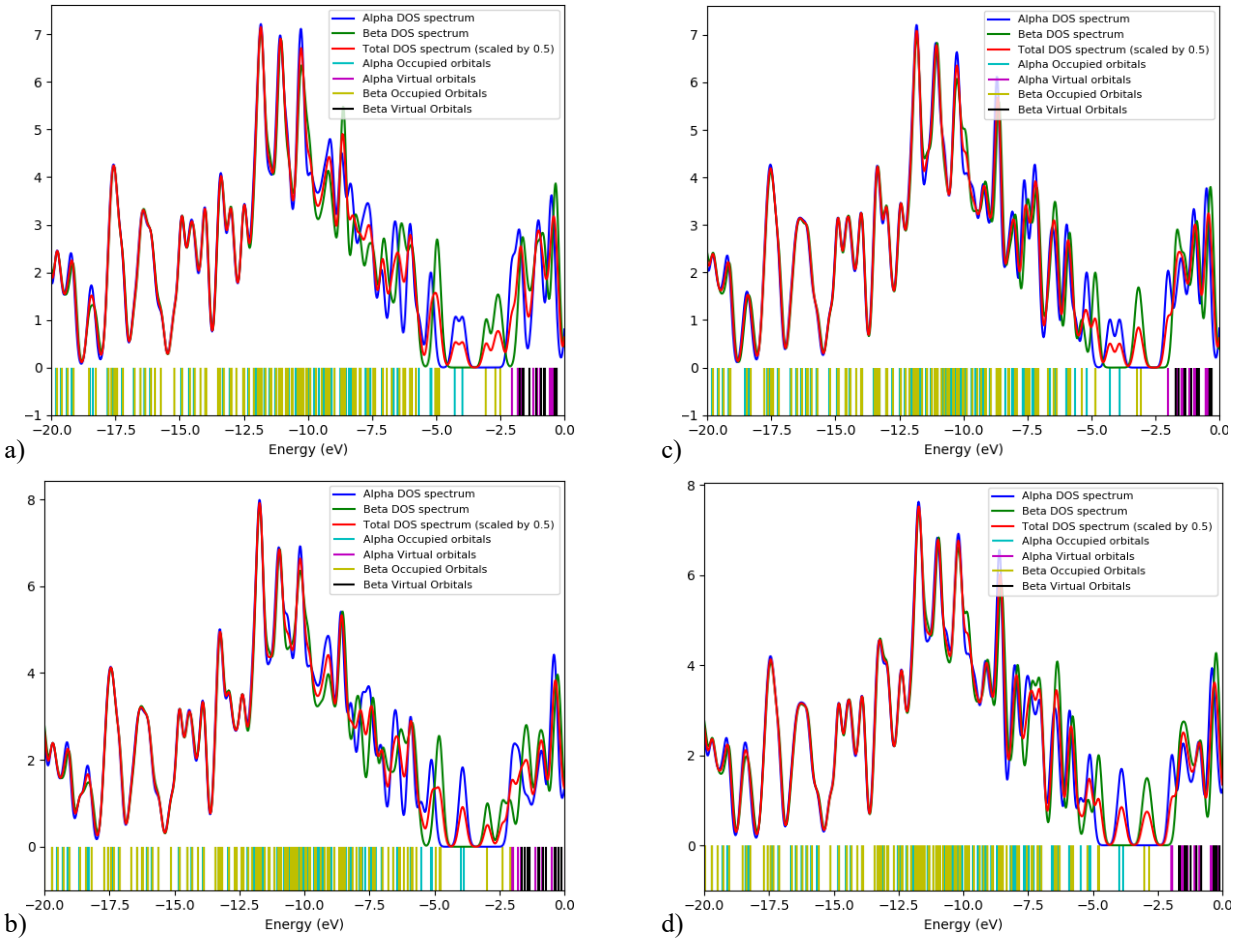


**Fig. 5** The DOS plots for optimized geometries of a) Fe-graphene structure and b) MM adsorbed on Fe-graphene structure, c) Co-graphene structure and d) MM adsorbed on Co-graphene structure.

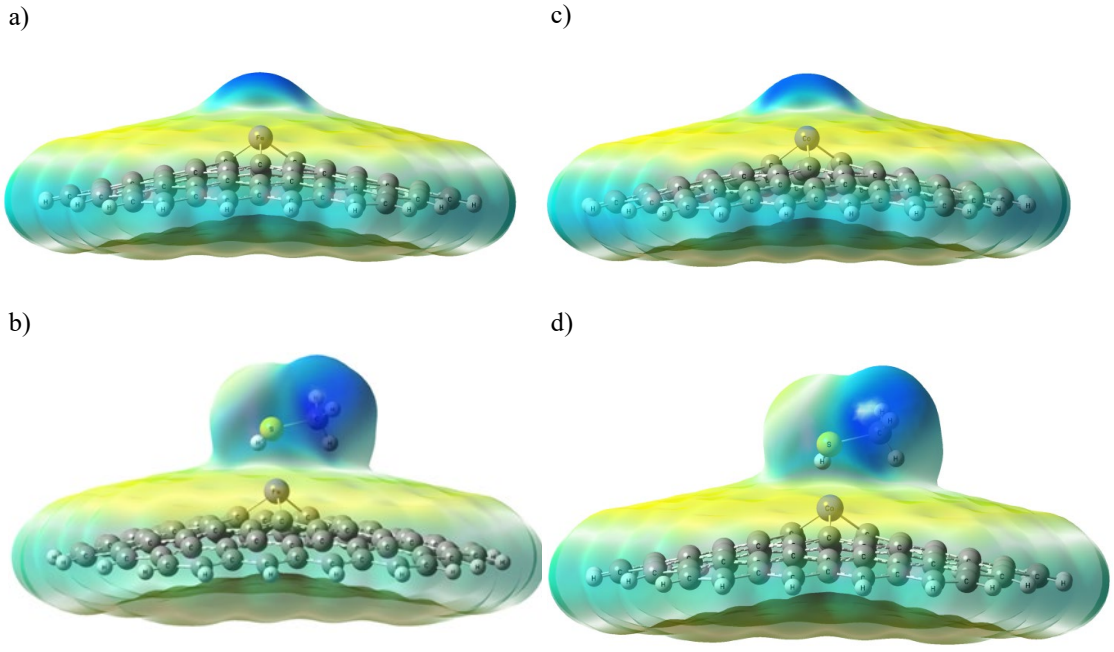


**Fig. 6** The ESP maps with projection of for the optimized geometries of a) Fe-graphene structure and b) MM adsorbed on Fe-graphene structure, c) Co-graphene structure and d) MM adsorbed on Co-graphene structure.

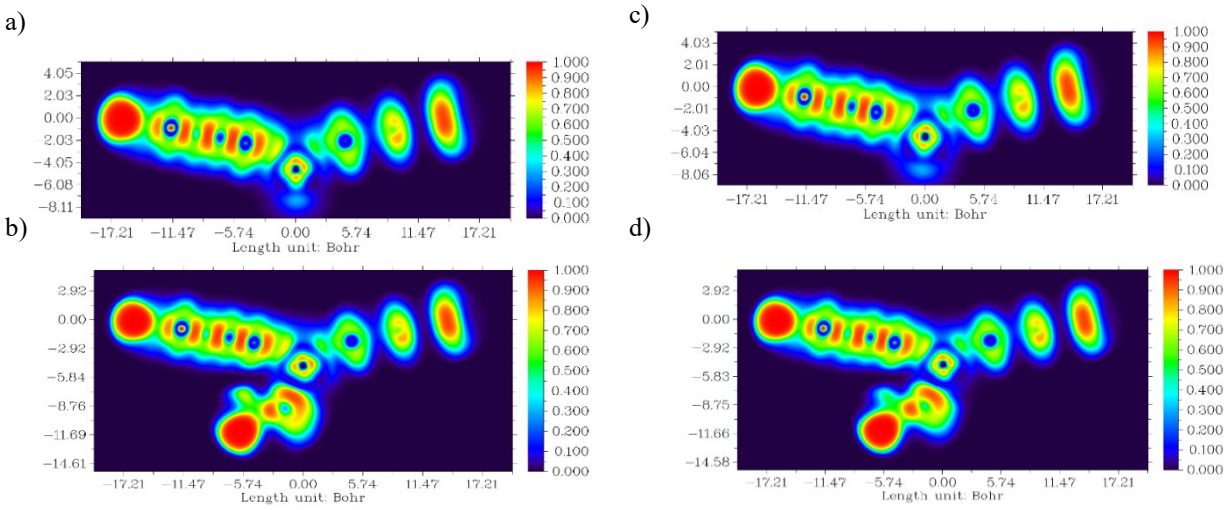


**Fig. 7** The ELF maps for the optimized geometries of a) Fe-graphene structure and b) MM adsorbed on Fe-graphene structure, c) Co-graphene structure and d) MM adsorbed on Co-graphene structure.

## 4. Conclusion

In present research, the sensor and adsorption abilities of Fe-graphene and Co-graphene structures toward MM molecule were examined by DFT method. After MM adsorption was performed on Fe-graphene and Co-graphene structures, some analysis was detaily made for structural and electronical properties. According to the adsorption energy values, Fe- and Co-graphene structures were found to be good adsorbent materials against the MM molecule and the adsorption processes were spontaneous. Mulliken charge distributions show that charge transfer between the adsorbed MM molecule and the Fe-doped graphene and Co-doped graphene structure has occurred. The Eg of the Fe-graphene structure substantially reduced upon MM adsorption, but the Eg of the Co-graphene structure increased. As a result of the improved electrical conductivity of the Fe-graphene structure, it has been revealed that it could be employed as an electronic sensor. Besides, it has been determined that there is no significant change in the work functions of the sensors and thus these structures cannot be Φ-type sensors.

## Acknowledgements

Acknowledgement: The numerical calculations reported in this paper were in part completed at ULAKBIM/TUBITAK, High Performance and Grid Computing Center (the resources of TRUBA)

## References

[1] S.S. Meshkat, O. Tavakoli, A. Rashidi, M.D. Esrafili, Adsorptive mercaptan removal of liquid phase using nanoporous graphene: Equilibrium, kinetic study and DFT calculations, Ecotoxicology and Environmental Safety 165 (2018) 533-539.

[2] J.M. Martínez-Magadán, R. Oviedo-Roa, P. García, R. Martínez-Palou, DFT study of the interaction between ethanethiol and Fe-containing ionic liquids for desulfuration of natural gasoline, Fuel Processing Technology 97 (2012) 24-29.

[3] D.K. Papayannis, A.M. Kosmas, N. Tsolakis, Computational study of ethanethiol conversion reactions catalyzed by acidic zeolites, Microporous Mesoporous Materials 262 (2018) 59-67.

[4] M. Vahedpour, F. Karami, J. Shirazi, Theoretical study on the mechanism and thermodynamic of methanethiol and ozone reaction, Computational and Theoretical Chemistry 1042 (2014) 41–48.

[5] J. Lu, H. Hao, L. Zhang, Z. Xu, L. Zhong, Y. Zhao, D. He, J. Liu, D. Chen, H. Pu, S. He, Y. Luo, The investigation of the role of basic lanthanum (La) species on the improvement of catalytic activity and stability of HZSM-5 material for eliminating methanethiol-(CH3SH), Applied Catalysis B: Environmental 237 (2018) 185-197.

[6] D. Zhang, M. Strawn, J.T. Novak, Z.W. Wang, Kinetic modeling of the effect of solids

retention time on methanethiol dynamics in anaerobic digestion, Water Research 138 (2018) 301-311.

[7] R. Bhuvaneswari, V. Nagarajan, R. Chandiramouli, Methyl and Ethyl mercaptan molecular adsorption studies on novel Kagome arsenene nanosheets - A DFT outlook, Physica B: Condensed Matter 586 (2020) 412135.

[8] M. Khalkhali, A. Ghorbani, B. Bayati, Study of adsorption and diffusion of methyl mercaptan and methane on FAU zeolite using molecular simulation, Polyhedron 171 (2019) 403-410.

[9] H. Heidari, S. Afshari, E. Habibi, Sensing properties of pristine, Al-doped, and defected boron nitride nanosheet toward mercaptans: a first-principles study, RSC Advances 5 (2015) 94201-94209.

[10] D. Cortés-Arriagada, N. Villegas-Escobar, D.E. Ortega, Fe-doped graphene nanosheet as an adsorption platform of harmful gas molecules (CO, CO2 , SO2 and H2S), and the co-adsorption in O2 environments, Applied Surface Science 427 (2018) 227-236.

[11] Z. Khodadadi, Evaluation of H2S sensing characteristics of metals–doped graphene and metals-decorated graphene: Insights from DFT study, Physica E: Low-dimensional Systems and Nanostructures 99 (2018) 261-268.

[12] T. Wang, D. Huang, Z. Yang, S. Xu, G. He, X. Li, N. Hu, G. Yin, D. He, L. Zhang, A Review on Graphene-Based Gas/Vapor Sensors with Unique Properties and Potential Applications, Nano-Micro Letters 8 (2016) 95-119.

[13] F. Hidalgo, A. Rubio-Ponce, C. Noguez, Tuning Adsorption of Methylamine and Methanethiol on Twisted-Bilayer Graphene, Journal of Physical Chemistry C 123 (2019) 15273-15283.

[14] Z. Gao, W. Yang, X. Ding, G. Lv, W. Yan, Support effects in single atom iron catalysts on adsorption characteristics of toxic gases (NO2, NH3, SO3 and H2S), Applied Surface Science 436 (2018) 585-595.

[15] Y. Tang, L. Pan, W. Chen, Z. Shen, C. Li, X. Dai, The formation of H 2S on metal-modified graphene under hydrogen environments, Composite Interfaces 23 (2016) 423-432.

[16] A. Shahmoradi, M. Ghorbanzadeh Ahangari, M. Jahanshahi, M. Mirghoreishi, E. Fathi, A. Hamed Mashhadzadeh, Removal of methylmercaptan pollution using Ni and Pt-decorated graphene: an ab-initio DFT study, Journal of Sulfur Chemistry 41 (2020) 593-604.

[17] H.P. Zhang, X.G. Luo, H.T. Song, X.Y. Lin, X. Lu, Y. Tang, DFT study of adsorption and dissociation behavior of H 2 S on Fe-doped graphene, Applied Surface Science 317 (2014) 511-506.

[18] F. Li, Y.H. Zhang, L.F. Han, Y.H. Xiao, D.Z. Jia, Z.H. Guo, Understanding dopant and defect effect on H2S sensing performances of graphene: A first-principles study, Computational Materials Science 69 (2013) 222-228.

[19] W. Kohn and L. J. Sham, Self-Consistent Equations Including Exchange and Correlation Effects, Physical Review E 14 (1965) A1133-A1138.

[20] M. J. Frisch, G. W. Trucks, H. B. Schlegel, G. E. Scuseria, M. A. Robb, J. R. Cheeseman, G. Scalmani, V. Barone, B. Mennucci, G. A. Petersson, H. Nakatsuji, M. Caricato, X. Li, H. P. Hratchian, A. F. Izmaylov, J. Bloino, G. Zheng, J. L. Sonnenberg, M. Hada, M. Ehara, K. Toyota, R. Fukuda, J. Hasegawa, M. Ishida, T. Nakajima, Y. Honda, O. Kitao, H. Nakai, T. Vreven, J. A. Montgomery, Jr., J. E. Peralta, F. Ogliaro, M. Bearpark, J. J. Heyd, E. Brothers, K. N. Kudin, V. N. Staroverov, T. Keith, R. Kobayashi, J. Normand, K. Raghavachari, A. Rendell, J. C. Burant, S. S. Iyengar, J. Tomasi, M. Cossi, N. Rega, J. M. Millam, M. Klene, J. E. Knox, J. B. Cross, V. Bakken, C. Adamo, J. Jaramillo, R. Gomperts, R. E. Stratmann, O. Yazyev, A. J. Austin, R. Cammi, C. Pomelli, J. W. Ochterski, R. L. Martin, K. Morokuma, V. G. Zakrzewski, G. A. Voth, P. Salvador, J. J. Dannenberg, S. Dapprich, A. D. Daniels, O. Farkas, J. B. Foresman, J. V. Ortiz, J. Cioslowski and D. J. Fox, Gaussian 09, Revision D.01, Gaussian, Inc., Wallingford CT, 2013.

[21] A.D. Becke, Density-functional exchange-energy approximation with correct asymptotic behavior, Physical Review A 38 (1988) 3098-3100.

[22] C. Lee, W. Yang, R.G. Parr, Development of the Colle-Salvetti correlation-energy formula into a functional of the electron density, Physical Review B 37 (1988) 785-789.

[23] R.G. Pearson, R.G. Pearson, Chemical hardness and density functional theory, Journal of Chemical Sciences 117 (2005) 369-377.

[24] N.M. O'Boyle, A.L. Tenderholt, K.M. Langner, Cclib: A library for package-independent computational chemistry algorithms, Journal of Computational Chemistry 29 (2008) 839–845.

[25] R.S. Mulliken, Electronic population analysis on LCAO-MO molecular wave functions, Journal of Chemical Physics 23 (1955) 1833-1840.

[26] M.W. Wong, Vibrational frequency prediction using density functional theory, Chemical Physics Letters 256 (1996) 391–399.

[27] T. Lu, F. Chen, Multiwfn: A multifunctional wavefunction analyzer, Journal of Computational Chemistry 33 (2012) 580–592

[28] M.F. Fellah, Pt doped (8,0) single wall carbon nanotube as hydrogen sensor: A density functional theory study, International Journal of Hydrogen Energy 44 (2019) 27010-27021.

[29] S. Demir, M.F. Fellah, A DFT study on Pt doped (4, 0) SWCNT: CO adsorption and sensing, Applied Surface Science 504 (2020) 144141.

[30] A. Ahmadi, N.L. Hadipour, M. Kamfiroozi, Z. Bagheri, Theoretical study of aluminum nitride nanotubes for chemical sensing of formaldehyde, Sensors Actuators B Chemical 161 (2012) 1025–1029.

[31] N.L. Hadipour, A. Ahmadi Peyghan, H. Soleymanabadi, Theoretical study on the Al-doped ZnO nanoclusters for CO chemical sensors, Journal of Physical Chemistry C 119 (2015) 6398–6404.

[32] M. Eslami, V. Vahabi, A. Ahmadi Peyghan, Sensing properties of BN nanotube toward carcinogenic 4-chloroaniline: A computational study, Physica E: Low-dimensional Systems and Nanostructures 76 (2015) 6-11.

[33] L. Li, J. Zhao, Defected boron nitride nanosheet as an electronic sensor for 4-aminophenol: A density functional theory study, Journal of Molecular Liquids 306 (2020) 112926.

[34] M. Li, Y. Wei, G. Zhang, F. Wang, M. Li, H. Soleymanabadi, A DFT study on the detection of isoniazid drug by pristine, Si and Al doped C70 fullerenes, Physica E: Low-dimensional Systems and Nanostructures 118 (2020) 113878.

[35] Y. Liu, C. Liu, A. Kumar, A selective NO sensor based on the semiconducting BC2N nanotubes: a computational study, Molecular Physics 118 (2020) 1798528.

[36] G. Makov, Chemical hardness in density functional theory, Journal of Physical Chemistry A 99 (1995) 9337-9339.

[37] P. Sjoberg, P. Politzer, Use of the electrostatic potential at the molecular surface to interpret and predict nucleophilic processes, Journal of Physical Chemistry A 94 (1990) 3959-3961.

[38] G. Yu, L. Lyu, F. Zhang, D. Yan, W. Cao, C. Hu, Theoretical and experimental evidence for rGO-4-PP Nc as a metal-free Fenton-like catalyst by tuning the electron distribution, RSC Advances 8 (2018) 3312-20.

[39] F. Teixidor, G. Barberà, A. Vaca, R. Kivekäs, R. Sillanpää, J. Oliva, C. Viñas, Are methyl groups electron-donating or electron-withdrawing in boron clusters? Permethylation of o-carborane, Journal of the American Chemical Society 127 (2005) 10158-10159.